Atmos. Chem. Phys., 22, 1081–1096, 2022
https://doi.org/10.5194/acp-22-1081-2022

Atmospheric Chemistry and Physics
Open Access
EGU

The importance of alkyl nitrates and sea ice emissions to atmospheric NO_x sources and cycling in the summertime Southern Ocean marine boundary layer

Jessica M. Burger[1], Julie Granger[2], Emily Joyce[3], Meredith G. Hastings[3], Kurt A. M. Spence[1], and Katye E. Altieri[1]

[1]Department of Oceanography, University of Cape Town, Rondebosch, 7701, South Africa
[2]Department of Marine Sciences, University of Connecticut, Groton, CT 06340, USA
[3]Department of Earth, Environmental and Planetary Sciences and Institute at Brown for Environment and Society, Brown University, Providence, RI 02906, USA

Correspondence: Jessica M. Burger (brgjes006@uct.ac.za)

Received: 22 June 2021 – Discussion started: 6 July 2021
Revised: 30 November 2021 – Accepted: 6 December 2021 – Published: 21 January 2022

Abstract. Atmospheric nitrate originates from the oxidation of nitrogen oxides ($NO_x = NO+NO_2$) and impacts both tropospheric chemistry and climate. NO_x sources, cycling and NO_x to nitrate formation pathways are poorly constrained in remote marine regions, especially the Southern Ocean, where pristine conditions serve as a useful proxy for the pre-industrial atmosphere. Here, we measured the isotopic composition ($\delta^{15}N$ and $\delta^{18}O$) of atmospheric nitrate in coarse-mode ($> 1\,\mu m$) aerosols collected in the summertime marine boundary layer of the Atlantic Southern Ocean from 34.5 to 70° S and across the northern edge of the Weddell Sea. The $\delta^{15}N$–NO_3^- decreased with latitude from −2.7 ‰ to −42.9 ‰. The decline in $\delta^{15}N$ with latitude is attributed to changes in the dominant NO_x sources: lightning at the low latitudes, oceanic alkyl nitrates at the mid-latitudes and photolysis of nitrate in snow at the high latitudes. There is no evidence of any influence from anthropogenic NO_x sources or equilibrium isotope fractionation. Using air mass back trajectories and an isotope mixing model, we calculate that oceanic alkyl nitrate emissions have a $\delta^{15}N$ signature of -21.8 ± 7.6 ‰. Given that measurements of alkyl nitrate contributions to remote nitrogen budgets are scarce, this may be a useful tracer for detecting their contribution in other oceanic regions. The $\delta^{18}O$–NO_3^- was always less than 70 ‰, indicating that daytime processes involving OH are the dominant NO_x oxidation pathway during summer. Unusually low $\delta^{18}O$–NO_3^- values (less than 31 ‰) were observed at the western edge of the Weddell Sea. The air mass history of these samples indicates extensive interaction with sea-ice-covered ocean, which is known to enhance peroxy radical production. The observed low $\delta^{18}O$–NO_3^- is therefore attributed to increased exchange of NO with peroxy radicals, which have a low $\delta^{18}O$, relative to ozone, which has a high $\delta^{18}O$. This study reveals that the mid- and high-latitude surface ocean may serve as a more important NO_x source than previously thought and that the ice-covered surface ocean impacts the reactive nitrogen budget as well as the oxidative capacity of the marine boundary layer.

Published by Copernicus Publications on behalf of the European Geosciences Union.

1 Introduction

Atmospheric nitrate (NO_3^-), hereafter defined as gas-phase nitric acid (HNO_3) and particulate NO_3^- (p-NO_3^-), impacts air quality and climate by contributing to atmospheric particulate matter (Park and Kim, 2005) and influencing the Earth's radiative heat budget (IPCC, 2013). It also plays a major role in the biogeochemical cycling of reactive nitrogen (Altieri et al., 2021). NO_3^- aerosols originate from the oxidation of nitrogen oxides, collectively referred to as NO_x ($NO_x = NO + NO_2$). NO_x cycling controls the chemical production of tropospheric ozone (O_3), a greenhouse gas and pollutant (Finlayson-Pitts and Pitts, 2000), which in turn contributes to the oxidizing capacity of the atmosphere (Alexander and Mickley, 2015). Globally, fossil fuel combustion is the primary NO_x source (van der A et al., 2008), which far exceeds natural emissions such as biomass burning (Finlayson-Pitts and Pitts, 2000), soil processes (Davidson and Kingerlee, 1997) and lightning (Schumann and Huntrieser, 2007).

Due to its remoteness, the summertime Southern Ocean marine boundary layer (MBL) can be representative of pre-industrial-like atmospheric conditions (Hamilton et al., 2014). The chemical composition of the Southern Ocean MBL is characterized by low NO_3^- concentrations (Virkkula et al., 2006), representative of a background aerosol environment (i.e. minimal anthropogenic influence). Furthermore, the South Atlantic sector of the Southern Ocean is primarily influenced by natural NO_x sources. During summer, high lightning activity over South America and southern Africa results in NO_x production between approximately 40° S and the intertropical convergence zone (ITCZ) (Nesbitt et al., 2000). As such, lightning is expected to be the dominant NO_x source in the low-latitude MBL (Schumann and Huntrieser, 2007; van der A et al., 2008). Because of its pristine nature, the summertime Southern Ocean serves as a unique region in which to study atmospheric chemistry and is a useful pre-industrial reference point for comparing the magnitude of anthropogenic aerosol impacts on climate (Haywood and Boucher, 2000; Hamilton et al., 2014).

The atmospheric chemistry of the polar MBL at the high southern latitudes differs from that of the mid- and low-latitude MBL. During summer, high levels of photochemistry result in the emission of reactive gases from sea ice and snow cover in the Antarctic. As a result, highly elevated concentrations of hydrogen oxide radicals (HO_x = OH + peroxy radicals), halogens, nitrous acid (HONO), and NO_x have been observed during spring and summer in the polar regions (Brough et al., 2019). Furthermore, photochemical production of NO_x within the surface snow of Antarctica and subsequent oxidation in the overlying atmosphere represents a significant NO_3^- source to the Antarctic troposphere (Jones et al., 2000, 2001). NO_3^- photolysis near the surface–air interface of ice crystals produces NO_2 (Grannas et al. 2007; Jones et al., 2000), which can be released to the firn (i.e. the intermediate stage of ice between snow and glacial ice) air and escape the snowpack to the overlying atmosphere (Erbland et al., 2013; Shi et al., 2015, 2018). During winter, additional NO_x sources to the Antarctic atmosphere may include long-range-transported peroxyacetyl nitrates (PAN) and stratospheric inputs (Savarino et al., 2007; Lee et al., 2014; Walters et al., 2019).

Emission of alkyl nitrates (a group of nitrogen gases collectively referred to as $RONO_2$) from the surface ocean have been recently proposed as a potential NO_x source to the MBL in remote regions (Williams et al., 2014; Fisher et al., 2018). Observations of elevated MBL alkyl nitrate concentrations suggest that a direct oceanic source exists in both the tropics (Atlas et al., 1993; Blake et al., 2003) and the high-latitude Southern Ocean (Blake et al., 1999; Jones et al., 1999). Although the exact mechanism remains unclear, experimental evidence suggests that oceanic $RONO_2$ production occurs via photochemical processes involving the aqueous-phase reaction of RO_2, derived from the photolysis of oceanic dissolved organic matter, and NO, derived from seawater nitrite photolysis (Dahl et al., 2003; Dahl and Saltzman, 2008). Supersaturated $RONO_2$ conditions in the surface ultimately drive a net flux from the ocean to the atmosphere (Chuck et al., 2002; Dahl et al., 2005). The photolysis of emitted $RONO_2$ and subsequent OH oxidation in the overlying atmosphere leads to NO_x formation (Fisher et al., 2018), and/or $RONO_2$ can form aerosol NO_3^- directly by hydrolysis (Rindelaub et al., 2015).

Current global atmospheric models suggest that oceanic $RONO_2$ represents a significant source of nitrogen (N) to the Southern Ocean MBL, accounting for 20 % to 60 % of the reactive N pool at high latitudes (60 to 90° S) (Fisher et al., 2018). However, only one shipborne dataset with coincident ocean–atmosphere $RONO_2$ concentration measurements exists to substantiate this notion (Hughes et al., 2008). Additionally, the NO_x source from $RONO_2$ degradation dominates relative to model-defined primary NO_x emission sources over the Southern Ocean, which include shipping, aircraft and lightning (Fisher et al., 2018). However, the lack of seawater observations available to constrain Southern Ocean $RONO_2$ distributions hampers the validation of model fluxes. Better understanding of the Southern Ocean $RONO_2$ source is required to improve simulations and accurately evaluate its contribution to the Southern Ocean MBL NO_x budget.

Natural abundance isotopes of atmospheric nitrate

Measurements of the oxygen (O) and N stable isotope ratios of atmospheric NO_3^- can be used to constrain NO_x sources, NO/NO_2 cycling and NO_x to NO_3^- oxidation pathways, which are critical for understanding the reactive N budget in the atmosphere. This technique has been applied in polluted (Elliott et al., 2007; Zong et al., 2017), open-ocean (Hastings et al., 2003; Morin et al., 2009; Kamezaki et al., 2019; Gobel et al., 2013; Altieri et al., 2013) and polar environments

(Morin et al., 2009; Walters et al., 2019). Stable isotope ratios are reported as a ratio of the heavy to light isotopologues of a sample relative to the constant isotopic ratio of a reference standard, using delta (δ) notation in units of per mil (‰) following Eq. (1):

$$\delta = \left(\left(R_{\text{sample}}/R_{\text{standard}}\right) - 1\right) \times 1000, \quad (1)$$

where R represents the ratio of $^{15}N/^{14}N$ or $^{18}O/^{16}O$ in the sample and in the reference standard, respectively. The reference for O is Vienna Standard Mean Ocean Water (VSMOW), and for N it is atmospheric N_2 (Bölhke et al., 2003).

When NO_x is converted to NO_3^-, the N atom is conserved. As such, it is generally expected that the N stable isotope ratio of atmospheric NO_3^- ($\delta^{15}N$–NO_3^-) reflects the $\delta^{15}N$ of the source NO_x (Kendall et al., 2007), plus any isotopic fractionation associated with NO/NO_2 cycling or NO_x to NO_3^- conversion. For example, the $\delta^{15}N$ of lightning generated NO_x is close to 0 ‰ (Hoering, 1957) and is distinct from stratospheric and snowpack NO_x. Savarino et al. (2007) used the degree of N_2O destruction in the stratosphere and the associated isotopic fractionation to derive an Antarctic stratospheric $\delta^{15}N$–NO_x source signature of 19 ± 3 ‰ (Savarino et al., 2007). In contrast, snow-emitted NO_x typically has a very low $\delta^{15}N$ signature due to the large fractionation ($^{15}\varepsilon$) of ~ -48 ‰ (Berhanu et al., 2014, 2015) associated with NO_3^- photolysis in the snowpack, where $^{15}\varepsilon = (\text{KIE}-1)\times 1000$ ‰, and the kinetic isotope effect (KIE) is the ratio of the rates with which the two isotopes of N are converted from reactant to product. If equilibrium isotope fractionation during NO/NO_2 cycling occurs, it results in the ^{15}N enrichment of NO_2 such that the NO_3^- formed from this NO_2 will have a higher $\delta^{15}N$–NO_3^- than the initial NO_x source (Freyer et al., 1993; Walters et al., 2016). Equilibrium isotope fractionation during the transformation of NO_x to NO_3^- also results in higher $\delta^{15}N$–NO_3^- compared to the original NO_x source (Walters and Michalski, 2015).

In contrast to N, the O stable isotope ratio of atmospheric NO_3^- ($\delta^{18}O$–NO_3^-) is reflective of the oxidants involved in NO_x cycling prior to NO_3^- formation, as well as the dominant NO_3^- formation pathway (Hastings et al., 2003; Michalski et al., 2003; Alexander et al., 2020). The O atoms of NO_x are rapidly exchanged with oxidizing agents in the atmosphere to produce NO_3^-. Tropospheric NO_x recycles rapidly with O_3 following the equations below:

$$NO + O_3 \rightarrow NO_2 + O_2 \quad (R1)$$

$$NO_2 + O_2 + h\nu \rightarrow NO + O_3. \quad (R2)$$

The oxidation of NO to NO_2 requires an atmospheric oxidant, typically O_3, throughout most of the troposphere (Reaction R1), while the breakdown of NO_2 back to NO is photolytic and requires light (Reaction R2). Therefore, under night-time/dark conditions, Reaction (R2) shuts down, and NO_x is comprised almost entirely of NO_2.

The dominant daytime sink for NO_x is the oxidation of NO_2 by OH, which produces HNO_3 via Reaction (R3), where M is a non-reacting molecule.

$$NO_2 + OH + M \rightarrow HNO_3 + M \quad (R3)$$

Under night-time/dark conditions, the photolytic production of OH cannot occur, and NO_2 is oxidized by O_3 (Reaction R4). HNO_3 is ultimately formed via the hydrolysis of dinitrogen pentoxide (N_2O_5), following Reactions (R5) and (R6).

$$NO_2 + O_3 \rightarrow NO_3 + O_2 \quad (R4)$$

$$NO_3 + NO_2 + M \rightleftharpoons N_2O_5(g) + M \quad (R5)$$

$$N_2O_5(g) + H_2O(l) + \text{surface} \rightarrow 2HNO_3(aq) \quad (R6)$$

NO_3 can also react with hydrocarbons (HC) (e.g. dimethylsulfide, DMS) to form HNO_3 following Reaction (R7).

$$NO_3 + HC/DMS \rightarrow HNO_3 + \text{products} \quad (R7)$$

Lastly, in regions with elevated halogen concentrations, NO_2 can be oxidized by reactive halogens, for example, bromine oxide (BrO), to form HNO_3 following Reactions (R8) and (R9).

$$NO_2 + BrO \rightarrow BrONO_2 \quad (R8)$$

$$BrONO_2 + H_2O + \text{surface} \rightarrow HNO_3 + HOBr \quad (R9)$$

Typically, aerosol $\delta^{18}O$–NO_3^- is interpreted as being determined by the dominant NO_x oxidation pathways, Reaction (R3) vs. Reaction (R4) to Reaction (R9). If some combination of Reactions (R4)–(R9) occurs, then O_3 is the main oxidant, whereas during Reaction (R3), one of the O atoms originates from OH. The OH radical exchanges with H_2O vapour in the troposphere; therefore the $\delta^{18}O$ of OH is a function of the $\delta^{18}O$ of H_2O vapour, which generally ranges from -27.5 ‰ to 0 ‰ in the subtropics and over the Southern Ocean (Michalski et al., 2012; Guilpart et al., 2017; Dar et al., 2020), and equilibrium isotope exchange between OH and H_2O (Walters and Michalski, 2016). In contrast, the $\delta^{18}O$ of tropospheric O_3 is much higher, the most recent estimate being 114.8 ± 10.4 ‰ (Vicars and Savarino, 2014). Therefore, a higher $\delta^{18}O$ for atmospheric NO_3^- reflects the increased influence of O_3 on NO_x to NO_3^- conversion (Reactions R4–R9), and the $\delta^{18}O$–NO_3^- is lower when Reaction (R3) is favoured, due to the lack of exchange of O atoms with O_3 (Hastings et al., 2003; Fang et al., 2011; Altieri et al., 2013).

Here, we present the concentration and isotopic composition of coarse-mode (> 1 µm) atmospheric NO_3^- collected in the MBL of the Southern Ocean between Cape Town, South Africa, and coastal Antarctica, as well as across the Weddell Sea gyre, during summer. Using air mass back trajectories, surface ocean nitrite measurements and the aerosol $\delta^{15}N$–

and $\delta^{18}O$–NO_3^-, we address (1) the major NO_x sources as well as the main oxidants in NO/NO_2 cycling and NO_x to NO_3^- conversion across a large latitudinal transect of the Atlantic Southern Ocean and within the Weddell Sea gyre and (2) the influence of sea ice and snowpack emissions on NO_x/NO_3^- chemistry in the high-latitude MBL.

2 Methods

2.1 Sample collection

Samples were collected on board the Research Vessel (R/V) *SA Agulhas II* during one cruise subdivided into three legs. Leg one refers to the southward voyage from Cape Town (33.9° S, 18.4° E) to Penguin Bukta (71.4° S, 2.5° W) in early summer (7 to 19 December 2018) as part of the South African National Antarctic Expedition's annual relief voyage (SANAE 58). Leg two is the Weddell Sea Expedition (WSE) from 4 January to 21 February 2019. All data were recorded in GMT. The WSE refers to the voyage west from Penguin Bukta to the northern edge of the Weddell Sea gyre to the Larsen C Ice Shelf, followed by a detour to King George Island before returning to the Weddell Sea and sailing back to Penguin Bukta. Leg three refers to the SANAE 58 return voyage north from Penguin Bukta to Cape Town in late summer (27 February to 15 March 2019). From here on, legs one, two and three will be referred to as early summer, the Weddell Sea and late summer, respectively.

Size-segregated atmospheric aerosols were collected on the ninth floor above the bridge (approximately 20 m above sea level), using a high-volume air sampler (HV-AS; Tisch Environmental). Air was pumped at an average flow rate of 0.82 $m^3\,min^{-1}$ through a five-stage cascade impactor (TE-235; Tisch Environmental), loaded with combusted (400 °C for 4 h) glass fibre filters (TE-230-GF; Tisch Environmental) that have a surface area of approximately 119 cm^2. Aerosol nitrate in the MBL is predominantly present in the coarse mode (> 1 µm); therefore only filter stages 1 through 4 were analysed, where the aerodynamical diameter of particles collected is as follows: stage 1 (> 7 µm), stage 2 (3 to 7 µm), stage 3 (1.5 to 3 µm) and stage 4 (1 to 1.5 µm).

A sector collector was used to restrict HV-AS activity to avoid contamination from ship stack emissions (Campbell Scientific Africa). The HV-AS only began operating if the wind was blowing at an angle less than 75° or greater than 180° from the bow of the ship for a minimum of 10 min at a speed of at least 1 $m\,s^{-1}$. Filters were removed from the cascade impactor inside a laminar flow cabinet (Air Science), placed in individual zip-sealed plastic bags and stored at −20 °C until analysis.

Given that the MBL of the Southern Ocean is characterized by low atmospheric NO_3^- concentrations, an attempt was made to ensure that at least 24 h of in-sector sampling had passed before filters were removed from the cascade impactor. However, this was not always possible as on occasion the filters had to be removed early to avoid contamination due to unusual ship manoeuvres or stagnant conditions. Therefore, sampling times ranged between 13 and 88 h across the three legs. The details of each cruise leg can be found in the Supplement (Table S1).

During the research voyage, a field blank was collected by fitting the cascade impactor with a set of filters and walking the cascade impactor from the laboratory to the HV-AS in the same way that atmospheric samples were deployed. The cascade impactor was placed into the HV-AS and then immediately removed without the HV-AS turning on, after which the filters were removed from the cascade impactor and stored in the same manner as the atmospheric samples. All chemical analyses performed on samples were also performed on the field blank filters to assess possible contamination during filter deployment or sample handling.

2.2 Sample analysis

Filter stages 1 to 4 were extracted using ultra-clean deionized water (DI; 18.2 MΩ) under a laminar flow cabinet (Air Science). The extraction ratio was approximately 30 cm^2 of filter in 25 mL of DI. Extracts were immediately sonicated for 1 h and then stored at 4 °C for at least 12 h. Thereafter, extracts were filtered (0.2 µm) using an acid-washed syringe into a clean 30 mL HDPE bottle and stored at −20 °C until analysis (Baker et al., 2010).

Aerosol nitrate concentrations ($[NO_3^-]$) were determined using a Thermo Scientific Dionex Aquion ion chromatography (IC) system (precision of ±0.3 $\mu mol\,L^{-1}$). The anion IC system contained an AG22 RFIC 4 × 50 mm guard column and AG22 RFIC 4 × 250 mm analytical column. A six-point standard curve that encompassed the range of sample concentrations (extract $[NO_3^-]$: 1.3 to 27.7 $\mu mol\,L^{-1}$) was run on each day of analysis (Dionex Seven Anion-II Standard), and an R^2 value > 0.999 was required for sample analysis to proceed. Final aerosol $[NO_3^-]$ was corrected by subtracting the field blanks, which represented 35 % of the total $[NO_3^-]$ on average. Aerosol samples were also analysed for $[NO_3^-]$ using a Lachat QuikChem® flow injection autoanalyzer (precision of ±0.8 $\mu mol\,L^{-1}$). The average $[NO_3^-]$ measured using the Lachat QuikChem® flow injection autoanalyzer and the IC system is reported (Table S3).

Nitrogen and oxygen isotopic ratios were measured using the denitrifier method (Sigman et al., 2001; Casciotti et al., 2002). To determine the $^{15}N/^{14}N$ and $^{18}O/^{16}O$ of NO_3^-, a natural strain of denitrifying bacteria, *Pseudomonas aureofaciens*, that lack the terminal nitrous oxide (N_2O) reductase enzyme, was used to convert aqueous NO_3^- quantitatively to N_2O gas. The product N_2O was analysed by continuous flow isotope ratio mass spectrometry using a Delta V Advantage isotope ratio mass spectrometer (IRMS) interfaced with an online N_2O extraction and purification system. Individual analyses were referenced to injections of N_2O from a pure gas cylinder and then standardized through com-

parison to the international reference materials of IAEA-N3 and USGS34 for $\delta^{15}N$–NO_3^- and IAEA-N3, USGS34 and USGS35 for $\delta^{18}O$–NO_3^- (Table S2) (Böhlke et al., 2003). The $^{15}N/^{14}N$ of samples was corrected for the contribution of ^{17}O to the peak at mass 45 using an average reported $\Delta^{17}O$ value of 26 ‰ from atmospheric nitrate collected in the Weddell Sea (Morin et al., 2009). The pooled standard deviation for all measurements of IAEA-N3 and USGS34 for $\delta^{15}N$–NO_3^- and IAEA-N3, USGS34 and USGS35 for $\delta^{18}O$–NO_3^- are reported (Table S2). All samples were measured in triplicate in separate batch analyses. The pooled standard deviation from all replicate analyses of samples was 0.25 ‰ for $\delta^{15}N$–NO_3^- and 0.64 ‰ for $\delta^{18}O$–NO_3^-. The average $\delta^{15}N$–NO_3^- and $\delta^{18}O$–NO_3^- computed for each filter deployment was weighted by the $[NO_3^-]$ observed for each stage, and error was propagated according to standard statistical practises (Table S3).

Seawater samples were collected in triplicate every 2 h from the ship's underway system (position at depth approximately 5 m) for the analysis of surface ocean nitrite concentrations ($[NO_2^-]$). $[NO_2^-]$ was analysed using the colorimetric method of Grasshoff et al. (1983) using a Thermo Scientific Genesys 30 visible spectrophotometer (detection limit of 0.05 µmol L^{-1}) (Table S4).

2.3 Air mass back trajectory analysis

To determine the air mass source region for each aerosol sample, air mass back trajectories (AMBTs) were computed for each hour in which the HV-AS was operational for at least 45 min of that hour. Given that the ship was moving, a different date, time and starting location were used to compute each AMBT. An altitude of 20 m was chosen to match the height of the HV-AS above sea level, and 72 h AMBTs were computed to account for the lifetime of NO_3^- in the atmosphere. All AMBTs were computed with NOAA's Hybrid Single-Particle Lagrangian Integrated Trajectory model (HYSPLIT v 4), using NCEP Global Data Assimilation System (GDAS) output, which can be accessed at https://www.arl.noaa.gov/ready/hysplit4.html (last access: 12 January 2022) (NOAA Air Resources Laboratory, Silver Spring, Maryland) (Stein et al., 2015; Rolph, 2016).

3 Results

The coarse-mode (> 1 µm in diameter) aerosol $[NO_3^-]$, computed by summing the $[NO_3^-]$ of stages 1 through 4, ranged from 17.3 to 264.0 ng m^{-3} (Fig. 1a and Table 1). The mass-weighted $\delta^{15}N$ of coarse-mode aerosol NO_3^- ranged from −43.1 ‰ to −2.7 ‰ (Figs. 1b, 2 and Table 1). There were no clear trends in atmospheric $[NO_3^-]$ or $\delta^{15}N$–NO_3^- with aerosol size (Table S5).

The highest nitrate concentrations occurred between 34 and 45° S, and then they decreased with increasing latitude (Fig. 1a). Similarly, higher values characterized $\delta^{15}N$–NO_3^- between 34 and 45° S (−4.9 ± 1.3 ‰), and then they decreased with increasing latitude (Fig. 1b). At high latitudes (south of 60° S), median values of 30.31 ng m^{-3} and −22.2 ‰ were observed for nitrate concentration and $\delta^{15}N$, respectively. Coincident mass-weighted $\delta^{18}O$–NO_3^- values ranged from 16.5 ‰ to 70 ‰ (Figs. 1c, 3 and Table 1). No latitudinal trend in $\delta^{18}O$–NO_3^- was apparent, although distinctly low $\delta^{18}O$–NO_3^- values were observed in the Weddell Sea, as discussed in Sect. 4.3 below. The difference between $\delta^{18}O$–NO_3^- observed in the Weddell Sea (during January to February) and $\delta^{18}O$–NO_3^- observed at corresponding latitudes (56 to 70° S) during the early and late summer transects is statistically significant (p value = 0.009). The early and late summer cruise transects were similar spatially in that both took place along the same hydrographic line (i.e. the Good Hope line), apart from the deviation to South Georgia during late summer (Fig. 2a, b). Even though the early and late summer cruise transects occurred in December and March, respectively, there is no statistically significant difference in $[NO_3^-]$ (p value = 0.43), $\delta^{15}N$–NO_3^- (p value = 0.53) or $\delta^{18}O$–NO_3^- (p value = 0.67) between them. Therefore, the early and late summer legs are discussed together and collectively referred to as the latitudinal transect.

4 Discussion

Our observations reveal a latitudinal gradient in atmospheric NO_3^- concentration and $\delta^{15}N$–NO_3^-, which we hypothesize may be attributed to the varying contribution of the dominant NO_x sources present between Cape Town and coastal Antarctica. In contrast, $\delta^{18}O$–NO_3^- depicts no latitudinal trend; however, relatively low $\delta^{18}O$–NO_3^- values are observed in the Weddell Sea, which we hypothesize may be attributed to the influence of sea ice emissions on NO_x cycling. Below, we first discuss the extent to which anthropogenic NO_x sources may influence the observed atmospheric NO_3^- concentrations and $\delta^{15}N$ signatures. Then we discuss the dominant NO_x sources to low-, mid- and high-latitude Southern Ocean MBL NO_3^-, determined in part from 72 h AMBTs, as well as the role of various oxidants in NO/NO_2 cycling and NO_2 oxidation.

4.1 Minimal influence of anthropogenic NO_x sources

Aerosol NO_3^- concentrations were low (< 100 ng m^{-3}; Fig. 1a) for most air masses sampled along the latitudinal transect and in the Weddell Sea, consistent with the expectation of minimal influence from anthropogenic NO_x sources. For comparison, $[NO_3^-]$ in a polluted urban airshed over South Africa can be > 500 ng m^{-3} (Collett et al., 2010). Interestingly, NO_3^- concentrations were higher (±200 ng m^{-3}; Fig. 1a) in samples collected near the South African coast at the beginning of the latitudinal transect (i.e. above 43° S). However, 72 h AMBTs computed for all latitudinal transect

Table 1. The average (avg), standard deviation (SD) and range of total coarse-mode (> 1 µm) atmospheric nitrate concentration ($[NO_3^-]$; ng m^{-3}) and the mass-weighted average N and O isotopic composition of coarse-mode nitrate ($\delta^{15}N$–NO_3^- and $\delta^{18}O$–NO_3^-; ‰) are shown. Cruise legs are denoted as follows: early summer (ES), Weddell Sea (WS) and late summer (LS).

Leg	$[NO_3^-]$ (ng m^{-3})		$\delta^{15}N$–NO_3^- (‰ vs. N_2)		$\delta^{18}O$–NO_3^- (‰ vs. VSMOW)	
	Avg (SD)	Range	Avg (SD)	Range	Avg (SD)	Range
ES	99.7 (72.8)	23.9 to 264.0	−19.5 (16.4)	−42.9 to −2.7	47.1 (17.8)	16.5 to 70.0
WS	33.8 (13.2)	17.3 to 67.3	−22.7 (7.2)	−38.1 to −11.6	38.4 (12.9)	18.8 to 60.3
LS	67.5 (61.4)	19.9 to 199.0	−15.0 (8.1)	−25.6 to −4.6	50.3 (6.3)	43.1 to 58.9

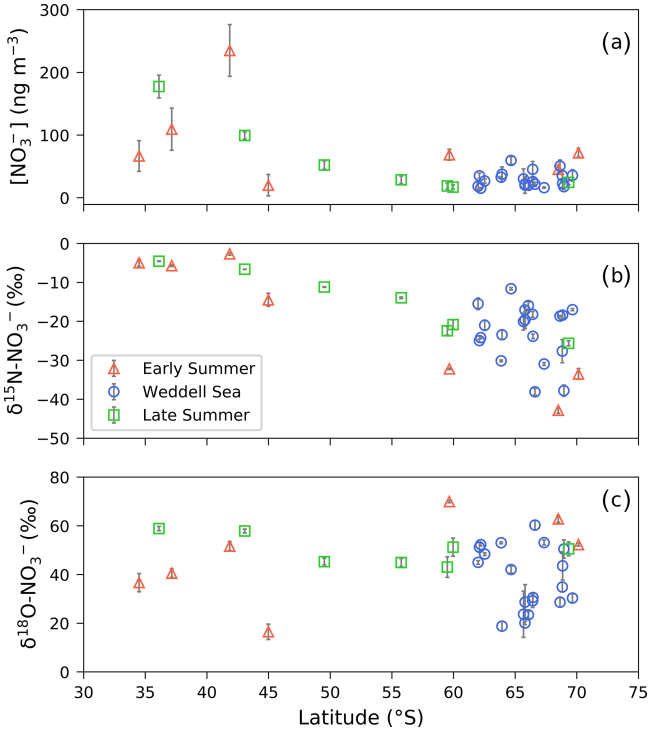

Figure 1. **(a)** The average (±1 SD) coarse-mode (> 1 µm) nitrate concentration $[NO_3^-]$ (ng m^{-3}) and the weighted average (±1 SD) $\delta^{15}N$ **(b)** and $\delta^{18}O$ **(c)** of atmospheric nitrate ($\delta^{15}N$–NO_3^- (‰ vs. N_2) and $\delta^{18}O$–NO_3^- (‰ vs. VSMOW), respectively), as a function of latitude (° S). Early and late summer latitudinal transects are denoted by the red triangles and green squares, respectively. Weddell Sea samples are denoted by blue circles. Where error bars (±1 SD) are not visible, the standard deviation is smaller than the size of the marker.

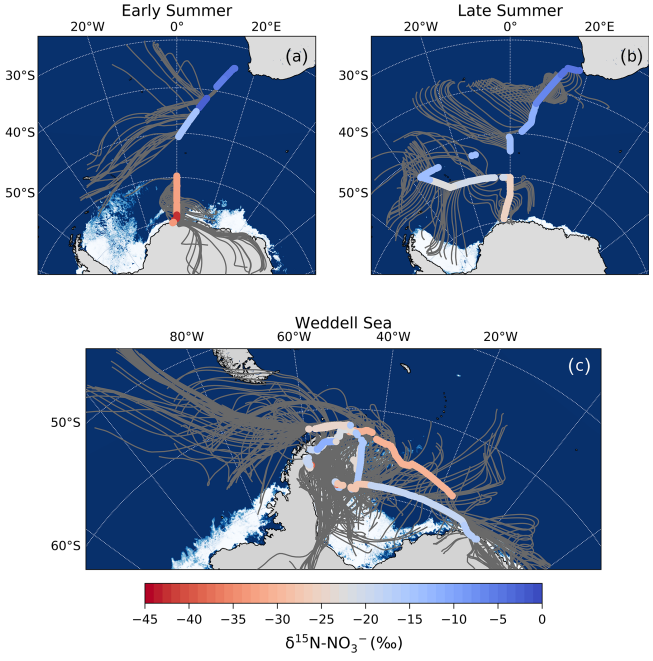

Figure 2. The 72 h AMBTs (grey lines) computed for each hour of the voyage when the HV-AS was operational for more than 45 min of the hour during early summer **(a)**, during late summer **(b)** and in the Weddell Sea **(c)**. The colour bar represents the weighted average $\delta^{15}N$ of coarse-mode (> 1 µm) atmospheric nitrate ($\delta^{15}N$–NO_3^-). Individual AMBTs for each aerosol sample from the Weddell Sea are shown in Fig. S1 in the Supplement. The white area represents the location of the sea ice determined using satellite-derived sea ice concentration data, obtained from passive microwave sensors AMSR2 (Advanced Microwave Scanning Radiometer 2; Spreen et al., 2008).

samples indicate that sampled air masses originated from over the South Atlantic sector of the Southern Ocean (Fig. 2a and b), with no continental influence and limited opportunity for direct anthropogenic NO_x emissions to contribute to aerosol NO_3^-, assuming NO_3^- has a lifetime of 72 h (Alexander et al., 2020). Furthermore, contamination from ship stack emissions was avoided using a sector collector to restrict HV-AS activity to certain wind directions (Sect. 2.1). As such, the higher atmospheric NO_3^- concentrations observed near South Africa are best explained by greater lightning NO_x production, which generally occurs between 40° S and the ITCZ during summer (Nesbitt et al., 2000; van der A et al., 2008).

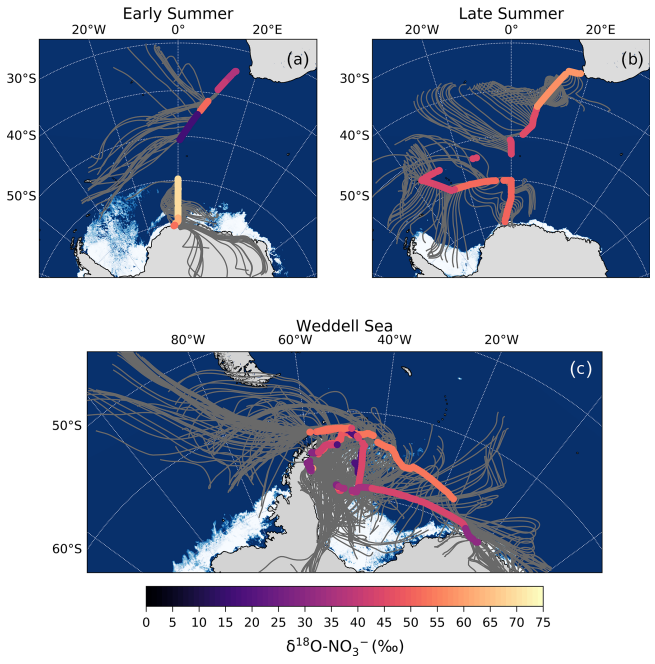

Figure 3. The 72 h AMBTs (grey lines) computed for each hour of the voyage when the HV-AS was operational for more than 45 min of the hour during early summer **(a)**, during late summer **(b)** and in the Weddell Sea **(c)**. The colour bar represents the weighted average $\delta^{18}O$ of coarse-mode (> 1 µm) atmospheric nitrate ($\delta^{18}O$–NO_3^-). Individual AMBTs for each aerosol sample from the Weddell Sea are shown in Fig. S1. The white area represents the location of the sea ice (see Fig. 2 caption).

4.2 Interpretation of natural NO_x sources using the N isotopic composition of atmospheric NO_3^-

Aerosol $\delta^{15}N$–NO_3^- ranged from −2.7 ‰ for low-latitude air masses to −42.9 ‰ for high-latitude air masses (including those sampled in the Weddell Sea; Fig. 1b). As discussed in Sect. 1.1, the $\delta^{15}N$–NO_3^- reflects the $\delta^{15}N$ of the source NO_x plus any isotopic fractionation imparted from NO/NO_2 cycling or NO_x to NO_3^- conversion. Similar to previous studies, we surmise that NO_x equilibrium fractionation is unlikely to be relevant in our system, as NO_x concentrations are significantly lower than O_3 concentrations (Elliott et al., 2007; Morin et al., 2009; Walters et al., 2016; Park et al., 2018). Typical O_3 concentrations observed at coastal sites in Antarctica are on the order of 20 ppbv (parts per billion by volume) (Nadzir et al., 2018), whereas the sum of NO and NO_2 rarely exceeds 0.04 ppbv (Jones et al., 2000; Weller et al., 2002; Bauguitte et al., 2012). Under these conditions NO_x isotopic exchange occurs at a much slower rate than Reactions (R1) and (R2), such that little to no equilibrium isotope fractionation is expressed, and the $\delta^{15}N$ of the NO_3^- should reflect the $\delta^{15}N$ of the NO_x source (Walters et al., 2016). Additionally, equilibrium isotope effects are temperature-dependent (increasing with decreasing temperature), and here ambient temperatures decline with increasing latitude. Therefore, if equilibrium isotope fractionation were occurring during NO/NO_2 cycling and/or NO_x to NO_3^- conversion, one would expect $\delta^{15}N$–NO_3^- to increase with latitude, as both fractionation processes produce NO_3^- with a higher $\delta^{15}N$ than the source NO_x. However, the opposite trend is observed here, whereby $\delta^{15}N$–NO_3^- decreases with increasing latitude (Fig. 1b). Therefore, we discount the hypothesis that equilibrium isotope effects can explain the latitudinal gradient in $\delta^{15}N$–NO_3^-.

NO_3^- in the Antarctic troposphere may also derive from stratospheric denitrification, whereby HNO_3 is injected into the troposphere from the stratosphere via the subsidence and penetration of polar stratospheric clouds (PSCs). However, this phenomenon typically occurs in winter when the tropospheric barrier is weak, and the lower stratosphere is cold enough for PSC formation (Savarino et al., 2007; Walters et al., 2019). Furthermore, $\delta^{15}N$–NO_3^- originating from stratospheric inputs is estimated to be 19 ± 3 ‰ (Savarino et al., 2007), a value substantially greater than the atmospheric $\delta^{15}N$–NO_3^- observed here for high-latitude air masses; thus, we discount a direct influence from stratospheric NO_x. We propose that the observed variation in atmospheric $\delta^{15}N$–NO_3^- across the Southern Ocean is best explained by the changing contribution of three dominant NO_x sources: lightning, surface ocean alkyl nitrate emissions and photochemical production on snow and ice, determined using AMBT analyses and typical NO_x source signatures where possible, as discussed below.

4.2.1 High latitudes: photochemical NO_x source

Aerosol $\delta^{15}N$–NO_3^- was relatively low in air masses from the southern high latitudes, including in the Weddell Sea (average of −24.3 ‰; Figs. 1b and 2). The latitudinal gradient in lightning NO_x production suggests that lightning NO_x is greatly reduced at high latitudes (Nesbitt et al., 2000). Similar to other studies in the region (Savarino et al., 2007; Morin et al., 2009), we suggest that photochemical NO_x production on snow or ice accounts for the low aerosol $\delta^{15}N$–NO_3^- in high-latitude air masses, where high-latitude air mass samples are defined as those exposed to the Antarctic continent or the surrounding sea ice (with sea ice concentration being at least 50 %). Antarctic estimates for isotopic fractionation associated with snow NO_3^- photolysis during summer range from −47.9 ‰ to −55.8 ‰ for laboratory and field experiments, respectively (Berhanu et al., 2014, 2015), resulting in the emission of low $\delta^{15}N$ NO_x to the overlying atmosphere (Savarino et al., 2007; Morin et al., 2009; Shi et al., 2018; Walters et al., 2019). Therefore, NO_3^- photolysis explains the very low $\delta^{15}N$–NO_3^- observed in high-latitude air masses in early and late summer that crossed snow-covered continental ice or sea ice before being sampled (Fig. 2a, b). During early summer, air masses spent significantly more time over the snow-covered continent compared to late summer, and

the sea ice extent was greater in early summer compared to late summer (Fig. 2a, b). Combined, these dynamics resulted in a much lower $\delta^{15}N$–NO_3^- for high-latitude air masses during early summer compared to late summer (minimum value of −42.9 ‰ vs. −25.6 ‰). Similarly low MBL $\delta^{15}N$–NO_3^- values (< −30 ‰) were recently observed for the southern high latitudes of the Indian Ocean (Shi et al., 2021). Our data are also consistent with year-round studies of atmospheric NO_3^- at coastal Antarctica (Savarino et al., 2007) and the South Pole (Walters et al., 2019), where $\delta^{15}N$–NO_3^- was reported to range from −46.9 ‰ to 10.8 ‰ and from −60.8 ‰ to 10.5 ‰, respectively. Both studies observed a seasonal cycle in $\delta^{15}N$–NO_3^-, whereby the lowest values occurred during sunlit periods (i.e. summer) due to snowpack NO_x emissions, and the highest values occurred during dark periods (i.e. winter) due to stratospheric inputs (Savarino et al., 2007; Walters et al., 2019).

4.2.2 Low latitudes to mid-latitudes: oceanic NO_x source

At the northern extent of our transects, the low-latitude aerosol samples, defined as those with air mass back trajectories originating from anywhere north of 43° S in early summer and 41° S in late summer (Fig. 2), had the highest average $\delta^{15}N$–NO_3^- signature (−4.9 ± 1.3 ‰; $n = 5$). These values can be attributed to lightning-generated NO_x, which has a $\delta^{15}N$ signature close to 0 ‰ (Hoering, 1957). Lightning activity at low latitudes is also consistent with the higher atmospheric [NO_3^-] observed (Fig. 1a) and is further supported by co-occurring high [NO_3^-] and relatively high $\delta^{15}N$–NO_3^- (Fig. S2). An average atmospheric $\delta^{15}N$–NO_3^- signature of −4 ‰ was previously reported for the low-latitude Atlantic Ocean, between 45° S and 45° N, and was similarly attributed to a combination of natural NO_x sources including lightning (Morin et al., 2009).

Aerosol samples across the mid-latitudes had an average $\delta^{15}N$–NO_3^- of −13.2 ‰ (Figs. 1b and 2). Mid-latitude air masses are defined as those originating from anywhere south of 43° S in early summer and south of 41° S in late summer that made no contact with Antarctica or any surrounding sea ice (Fig. 2a, b). Furthermore 43° S and 41° S represent the latitudes at which non-zero sea surface nitrite concentrations began to be observed in early and late summer (Fig. 4). Mid-latitude samples were therefore unlikely to be influenced by snow-emitted NO_x with its light isotopic signature. However, the observed aerosol $\delta^{15}N$–NO_3^- was too low (−14.5 ‰ to −11.2 ‰) to be explained solely by lightning-generated NO_x. In the absence of any signature of anthropogenic NO_x emissions (Sect. 4.1), we argue that the dominant NO_x source for the mid-latitude samples originates from seawater.

As mentioned in Sect. 1, the most likely mechanism for an oceanic NO_x source is via the photolysis of surface ocean derived $RONO_2$ in the MBL. NO derived from seawater nitrite is thought to limit $RONO_2$ production (Dahl and Saltzman, 2008; Dahl et al., 2012), such that non-zero nitrite concentrations are required for $RONO_2$ production to occur. Here, surface ocean nitrite concentrations were relatively high, in particular from ∼ 41 to 50° S (Fig. 4). Furthermore, the latitudinal extent of mid-latitude air masses with low $\delta^{15}N$–NO_3^- signatures corresponds well with the same latitudinal extent in which non-zero surface ocean nitrite concentrations occurred (Fig. 4). As such, we suggest that in this region oceanic $RONO_2$ emission is the main source to the Southern Ocean MBL, ultimately resulting in the low $\delta^{15}N$–NO_3^- values observed for mid-latitude air masses.

No estimates exist for the $\delta^{15}N$ of oceanic $RONO_2$; however $RONO_2$ photolysis may yield isotopically light NO_x given that NO_3^- photolysis produces low $\delta^{15}N$ products (e.g. Frey et al., 2009). Therefore, once oxidized in the overlying atmosphere, NO_x derived from oceanic $RONO_2$ photolysis may form atmospheric NO_3^- with a low $\delta^{15}N$ signature. Aerosol $\delta^{15}N$–NO_3^- values have been observed to range from −14.1 ‰ to −7.3 ‰ in the eastern equatorial Pacific (Kamezaki et al., 2019) and from −6 ‰ to ∼ 0 ‰ (average = −3.4 ‰) in the western equatorial Pacific (Shi et al., 2021). Observed $\delta^{15}N$–NO_3^- is higher in the western compared to the eastern equatorial Pacific, which could be attributed to the proximity of the western equatorial Pacific to continental/anthropogenic NO_x sources, resulting in NO_3^- having a higher $\delta^{15}N$ signature. The low average $\delta^{15}N$–NO_3^- observed for the mid-latitude air masses of the Southern Ocean MBL sampled in the present study (−14.5 ‰ to −11.2 ‰) is remarkably similar to that for the air masses observed in the eastern equatorial Pacific (Kamezaki et al., 2019). Kamezaki et al. (2019) also concluded that such low $\delta^{15}N$–NO_3^- values cannot be explained solely by lightning NO_x, and given the lack of considerable influence from any continental NO_x sources, they invoked the contribution of oceanic N emissions in the form of ammonia (NH_3) and/or $RONO_2$. However, NH_3 flux data for the summertime Atlantic Southern Ocean derived from in situ ocean/atmosphere observations suggest that the ocean in this region is a net sink of NH_3 (Altieri et al., 2021).

The latitudinal extent of our sampling campaign enabled us to estimate a range of likely values for the N isotopic composition of NO_3^- derived from oceanic $RONO_2$. We split the latitudinal transect into three regions, each characterized by the dominance of a different natural source of NO_3^-, i.e. lightning NO_x at low latitudes (Fig. 5, light orange), oceanic $RONO_2$ emissions at mid-latitudes (Fig. 5, dark orange) and snowpack emissions at high latitudes (Fig. 5, red).

Assuming that the dominant natural source of NO_3^- is the only source relevant in each latitudinal zone, we estimate the contribution of each source to total NO_3^- formation by ascertaining the amount of time air masses spent in each zone. We further assume that atmospheric $\delta^{15}N$–NO_3^- reflects at most a combination of two sources based on the AMBTs of each sample, either lightning NO_x and oceanic $RONO_2$ emissions

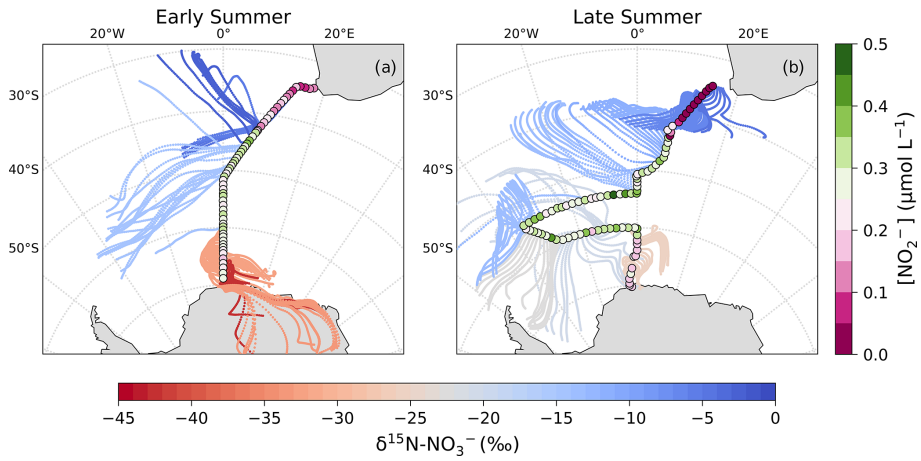

Figure 4. The 72 h AMBTs computed for each hour of the voyage during early **(a)** and late **(b)** summer, when the HV-AS was operational for more than 45 min of the hour. AMBTs are colour-coded by the weighted average δ^{15}N of atmospheric nitrate (δ^{15}N–NO_3^-), represented by the horizontal colour bar. Overlaid are the surface ocean nitrite concentrations (circles; $[NO_3^-]$; µmol L^{-1}), measured along each transect and represented by the vertical colour bar.

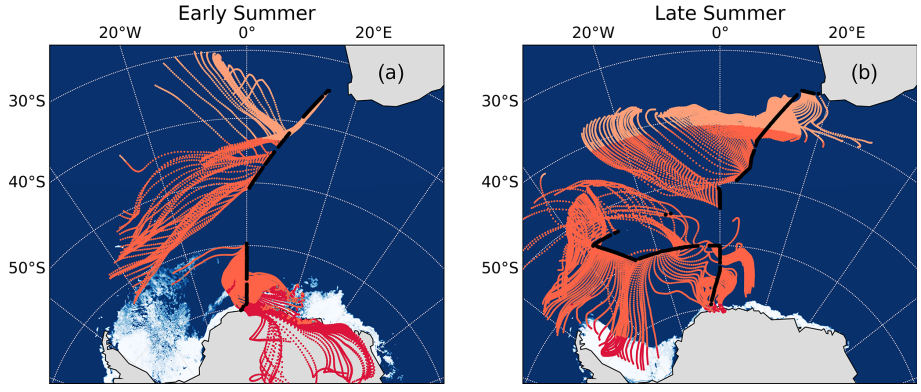

Figure 5. The 72 h AMBTs computed for each hour of the voyage during early **(a)** and late **(b)** summer, when the HV-AS was operational for more than 45 min of the hour. Light orange, dark orange and red AMBTs represent time spent over the low-, mid- and high-latitude Southern Ocean, respectively. The white area represents the location of the sea ice (see Fig. 2 caption).

near South Africa or oceanic $RONO_2$ emissions and snowpack NO_x emissions near Antarctica (Fig. 5 and Table S6). Using a two-endmember mixing model, the δ^{15}N signature of the source NO_3^- derived from mid-latitude Southern Ocean $RONO_2$ emissions was calculated for all samples where air masses from the mid-latitude region contributed at least 10 % (Table S6). This 10 % threshold was chosen as the isotopic endmember of oceanic $RONO_2$ is harder to determine with confidence when its contribution to total NO_3^- is less than 10 %.

As an example, the AMBTs for sample ES 4 spent 3 % of the time in the low-latitude zone and 97 % in the mid-latitude zone. Using the measured δ^{15}N–NO_3^- for ES 4 of −14.5 ‰, and assuming lightning NO_x has a δ^{15}N signature of 0 ‰, we calculate the δ^{15}N signature of the $RONO_2$-derived NO_3^- to be −14.9 ‰. It is important to note that using this approach to estimate the δ^{15}N–NO_3^- from oceanic $RONO_2$ emissions relies heavily on AMBTs generated using HYSPLIT. While HYSPLIT is a frequently used tool for assessing air mass origin in the Southern Hemisphere and over Antarctica (Morin et al., 2009; Walters et al., 2019; Shi et al., 2021), it is important to note that a spatial uncertainty of 15 % to 30 % of the trajectory path distance can be expected (Scarchilli et al., 2011). AMBTs also become increasingly uncertain the further back in time they are used (Sinclair et al., 2013). Some of this uncertainty is alleviated by the fact that the AMBTs generated here are relatively short (< 5 d). Additionally, the spatial scale of the low-, mid- and high-latitude zones is large, such that some variation in sample AMBTs will not significantly alter the expected dominant NO_3^- source.

Using this approach for each filter deployment along the latitudinal transect, an average δ^{15}N–NO_3^- from oceanic $RONO_2$ emissions of -21.8 ± 7.6 ‰ was estimated. Further-

more, the contribution of $RONO_2$ emissions can explain the lowering of $\delta^{15}N$ from 0 ‰ for the low-latitude air mass samples. For example, the highest $\delta^{15}N$ observed in the study was −2.7 ‰, and this sample has a < 5 % contribution from the mid-latitude zone. The other two low-latitude samples have 30 % to 40 % contribution from the mid-latitude zone, and their $\delta^{15}N$ is lower (Table S3), as expected due to the influence of $RONO_2$ emissions.

The influence of low $\delta^{15}N$–NO_3^- from $RONO_2$ emissions is not limited to the Southern Ocean, and this estimate of the N isotopic composition for the $RONO_2$ derived NO_3^- source may be useful to constrain the contribution of $RONO_2$ emissions to NO_3^- formation in other ocean regions with elevated surface ocean nitrite concentrations, such as the tropical Pacific.

4.3 The O isotopes of atmospheric nitrate

The corresponding $\delta^{18}O$ values allow us to determine the pathways of NO_3^- formation from NO_x. However, an assumption must first be made regarding the oxidation of NO to NO_2. While the dominant oxidant of NO to NO_2 is O_3 (Reaction R1) in most of the troposphere, over the open ocean there can be a significant contribution via the reaction of NO with peroxy radicals (HO_2 and its organic homologues RO_2) (Alexander et al., 2020). Peroxy radicals compete with O_3 to convert NO into NO_2 via Reaction (R10).

$$NO + HO_2(\text{or } RO_2) \rightarrow NO_2 + OH(\text{or } RO) \quad \text{(R10)}$$

The $\delta^{18}O$ of peroxy radicals is much lower than that of O_3 because the O atoms derive from atmospheric O_2, which has a well-defined $\delta^{18}O$ of 23.9 ‰ (Kroopnick and Craig, 1972). The $\delta^{18}O$–NO_2 can then be calculated using Eq. (2):

$$\delta^{18}O\text{–}NO_2 = (\delta^{18}O\text{–}O_2)(1-f) + (\delta^{18}O\text{–}O_3^*)(f), \quad (2)$$

where f is the fraction of NO_2 formed from Reaction (R1), $(1-f)$ is the fraction formed from Reaction (R10) and the terminal $\delta^{18}O$–O_3 value ($\delta^{18}O$–O_3^*) is 130.4±12.9 ‰ (Vicars and Savarino, 2014).

The $\delta^{18}O$–NO_3^- is then determined using Eq. (3), in which two-thirds of the O atoms in NO_3^- come from NO_2, and one-third comes from OH, i.e. Reaction (R3), or using Eq. (4), in which three-sixths of the O atoms in NO_3^- come from O_3, two-sixths come from NO_2 and one-sixth comes from H_2O, i.e. Reactions (R4)–(R6) (Hastings et al., 2003; Alexander et al., 2020).

$$\delta^{18}O\text{–}NO_{3\,(R3)}^- = (2/3)(\delta^{18}O\text{–}NO_2) + (1/3)(\delta^{18}O\text{–}OH) \quad (3)$$

$$\delta^{18}O\text{–}NO_{3\,(R4-R6)}^- = (1/2)(\delta^{18}O\text{–}O_3^*) + (1/3)(\delta^{18}O\text{–}NO_2) + (1/6)(\delta^{18}O\text{–}H_2O) \quad (4)$$

We assume that 15 % of NO to NO_2 conversion occurs via HO_2/RO_2 oxidation and 85 % by O_3 oxidation, as is suggested by global models (Alexander et al., 2020), and use the minimum and maximum $\delta^{18}O$–H_2O range of −27.5 ‰ to 0 ‰, the temperature-dependent equilibrium isotope exchange between OH and H_2O (Walters and Michalski, 2016) and the resulting minimum and maximum estimates for $\delta^{18}O$–OH of −67.4 ‰ to −41.0 ‰. Using these assumptions and Eqs. (3) and (4), the expected $\delta^{18}O$–NO_3^- for the daytime OH oxidation pathway (Reaction R3) is 46.5 ‰ to 71.4 ‰, and for the dark Reactions (R4)–(R6), it is 88.7 ‰ to 113.5 ‰.

The observed $\delta^{18}O$–NO_3^- values were all less than 70 ‰ (Figs. 1c and 3), suggesting that NO_x oxidation by OH (Reaction R3) was indeed the dominant pathway for atmospheric NO_3^- formation during summer. The low $\delta^{18}O$–NO_3^- values observed suggest a minimal influence of O_3 in the oxidation chemistry, ruling out both the halogen-related (Reactions R8 to R9) and DMS-related (Reaction R7) NO_3^- formation pathways in addition to N_2O_5 hydrolysis (Reactions R4 to R6). This is consistent with previous year-round studies of atmospheric NO_3^- at coastal Antarctica (Savarino et al., 2007) and the South Pole (Walters et al., 2019), where $\delta^{18}O$–NO_3^- was at a minimum in summer (59.6 ‰ and 47.0 ‰, respectively). Both studies confirm the importance of HO_x oxidation chemistry in summer when solar radiation enhances the production of these oxidants, followed by a switch to O_3-dominated oxidation chemistry in winter (Savarino et al., 2007; Ishino et al., 2017; Walters et al., 2019).

Interestingly, most aerosol samples have a $\delta^{18}O$–NO_3^- less than 46.5 ‰ ($n = 19$), the lower limit estimated above for the OH pathway. This suggests that there is more NO to NO_2 conversion via HO_2/RO_2 oxidation occurring than the global average. A maximum HO_2/RO_2 contribution to NO oxidation of ∼ 63 % is required to explain the lowest $\delta^{18}O$–NO_3^- value, which was observed over the mid-latitudes during early summer. Increased RO_2 production over the mid-latitudes could derive from $RONO_2$ photolysis in the MBL, which we hypothesize is happening in this region based on the $\delta^{15}N$–NO_3^- (Sect. 4.2.2).

Although the lowest $\delta^{18}O$ observation occurred in the mid-latitudes, the majority of low $\delta^{18}O$–NO_3^- values were observed in the Weddell Sea, away from the region of maximum $RONO_2$ emissions. Approximately half of the Weddell Sea samples have a $\delta^{18}O$–NO_3^- < 31 ‰, which would require a HO_2/RO_2 contribution to NO oxidation upwards of 40 % (more than double the contribution estimated by global models; Alexander et al., 2020). These $\delta^{18}O$–NO_3^- observations are unusually low compared to previous observations for the same region in spring (Morin et al., 2009).

We hypothesize that the large contribution of HO_2/RO_2 to NO/NO_2 oxidation (i.e. a decrease in f in Eq. 2) resulting in these low $\delta^{18}O$–NO_3^- values is due to the influence of sea ice emissions. The 72 h AMBTs for these low $\delta^{18}O$–NO_3^- Weddell Sea samples indicate that all the air masses

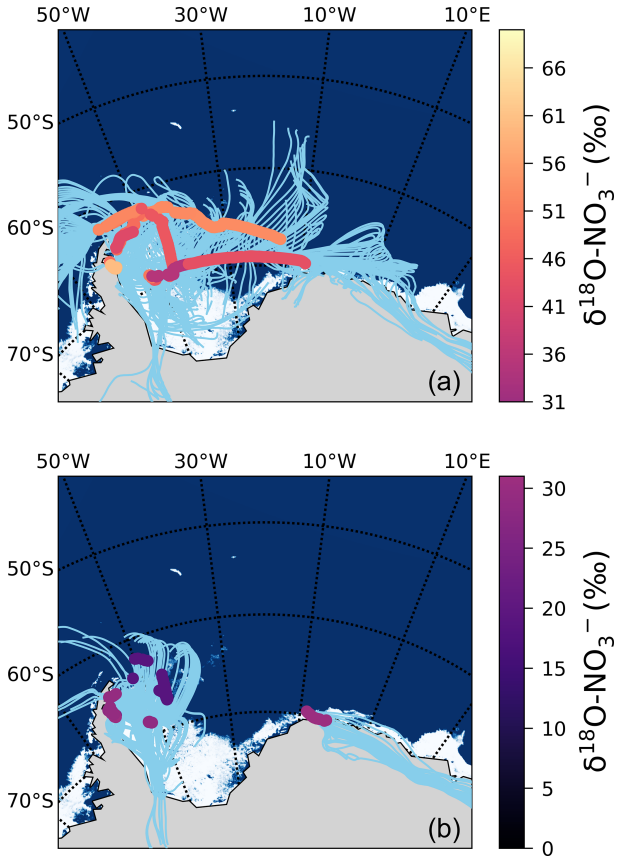

Figure 6. The 72 h AMBTs (light blue lines) computed for each hour of the voyage in the Weddell Sea, when the HV-AS was operational for more than 45 min of the hour. The vertical colour bar represents the weighted average $\delta^{18}O$ of atmospheric nitrate ($\delta^{18}O$–NO_3^-), where $\delta^{18}O$–NO_3^- was $> 31‰$ **(a)** and $< 31‰$ **(b)**. The white area represents the location of the sea ice (see Fig. 2 caption).

either originated from, or spent a significant amount of time recirculating, over the sea-ice-covered region of the western Weddell Sea (Fig. 6b). By contrast, aerosol samples from the Weddell Sea with $\delta^{18}O$–NO_3^- values greater than 31 ‰ have air masses that experienced significantly more oceanic influence (Fig. 6a).

There is evidence that sea ice can lead to enhanced peroxy radical production (Brough et al., 2019). In that work, increased $HO_2 + RO_2$ concentrations were observed during spring at a coastal Antarctic site when air masses arrived from across a sea-ice-covered zone. This was attributed to the oxidation of hydrocarbons by chlorine atoms, which leads to increased RO_2 concentrations via Reactions (R11) and (R12).

$$RH + Cl \rightarrow R + HCl \quad \text{(R11)}$$

$$R + O_2 \rightarrow RO_2 \quad \text{(R12)}$$

Cl atoms are much more reactive with hydrocarbons than OH (Monks, 2005) and can enhance hydrocarbon oxidation, even when present at low concentrations. Brough et al. (2019) suggest that air masses that traversed the sea ice zone contained photolabile chlorine compounds that built up at night until photolysis occurred during the next day (Brough et al., 2019). Although our study was conducted in summer (the season of minimum sea ice extent), the sampling locations were uniquely positioned at the western edge of the Weddell Sea gyre, where significant sea ice remained (Fig. 6). Therefore, we suggest that chlorine chemistry over the sea ice increased RO_2 concentrations at the time of our sampling, allowing the $NO + RO_2$ pathway to play a more significant role in the Weddell Sea and resulting in low $\delta^{18}O$–NO_3^- values. We note that the only other estimates of $\delta^{18}O$–NO_3^- from the Weddell Sea ranged from $\sim 50‰$ to 110 ‰ during springtime, and these samples were associated with air masses that spent almost no time over the sea ice and therefore had limited potential for this peroxy radical chemistry to drive down the $\delta^{18}O$–NO_3^- to the low values we observe (Morin et al., 2009).

5 Conclusions

Our observations across a large latitudinal gradient of the summertime Southern Ocean MBL suggest it is dominated by natural NO_x sources with distinct isotopic signatures. Aerosol NO_3^- was predominantly formed from lightning-generated NO_x with a $\delta^{15}N$ of $\sim 0‰$ at the lower latitudes, whereas snowpack NO_x emissions with a $\delta^{15}N \sim -48‰$ dominated the MBL inventory at higher latitudes. Over the mid-latitudes, NO_3^- derived primarily from oceanic $RONO_2$ emissions, with an estimated $\delta^{15}N$ signature of $\sim -22.0‰$. Additional research is needed to improve our mechanistic and isotopic understanding of surface ocean $RONO_2$ formation, flux and conversion to aerosol nitrate in order to constrain the contribution of oceanic $RONO_2$ emissions to NO_3^- formation in other ocean regions where this source has been invoked, such as the tropical Pacific (Kamezaki et al., 2019). The isotopic composition of NO_3^- observed here can further inform interpretations of Antarctic ice core NO_3^- isotope records to understand aerosol climate forcing and controls on the atmospheric oxidation budget over millennia (Freyer et al., 1996; Jiang et al., 2019) – the interpretation of which relies on knowledge of the NO_x isotopic source signatures in the polar atmosphere.

The $\delta^{18}O$–NO_3^- values were consistently lower than 70 ‰, which confirms NO_x oxidation by OH (Reaction R3) to be the dominant pathway for atmospheric NO_3^- formation during summer. However, unusually low $\delta^{18}O$–NO_3^- values observed at the mid-latitudes and in the Weddell Sea indicate the increased importance of peroxy radicals (and decreased importance of O_3) in NO oxidation to NO_2 in the MBL. At mid-latitudes, peroxy radicals (RO_2) may derive from

$RONO_2$ photolysis, while in the Weddell Sea, sea ice appears to play an important role in the formation of this oxidant via its influence on chlorine chemistry (Brough et al., 2019). This implies that snow-covered sea ice is not only a source of NO_x but also other species that have the potential to change the composition of the atmosphere above the ice and impact NO_x oxidation chemistry. These results also highlight the utility of $\delta^{18}O$–NO_3^- to identify the major oxidants in NO oxidation, as well as NO_x to NO_3^- conversion. In particular, $\delta^{18}O$–NO_3^- can serve as a useful tool for testing our understanding of the relative importance of HO_2/RO_2 in NO/NO_2 cycling, which can be difficult to constrain in some environments.

Our study challenges the traditional paradigm that considers the ocean to be a passive recipient of N deposition, as the Southern Ocean mid-latitude NO_3^- source may derive almost entirely from oceanic $RONO_2$ emissions. In the tropical equatorial Pacific atmosphere, Kamezaki et al. (2019) also suggested evidence for a low $\delta^{15}N$–NO_3^- source derived from the ocean. In the subtropical Atlantic Ocean MBL, Altieri et al. (2016) found that biogeochemical cycling in the surface ocean can directly influence the lower atmosphere, serving as a source of aerosol organic N and ammonium. This study suggests that the surface waters of the Southern Ocean may also serve as a NO_x source, ultimately resulting in NO_3^- aerosol formation. As such, the surface ocean may play a bigger role in atmospheric oxidative capacity over remote marine regions than previously thought.

Data availability. Datasets for this research are available at https://doi.org/10.5281/zenodo.5840260 (Burger et al., 2021).

Supplement. The supplement related to this article is available online at: https://doi.org/10.5194/acp-22-1081-2022-supplement.

Author contributions. KEA designed the study and sampling campaign, acquired funding and supervised the research. KEA and JG provided financial and laboratory resources and assisted in data validation. KAMS and JMB conducted the sampling at sea, and JMB performed the laboratory analyses. MGH and EJ assisted in data validation, reviewing and editing of the manuscript. JMB analysed the data and prepared the manuscript with contributions from all co-authors.

Competing interests. The contact author has declared that neither they nor their co-authors have any competing interests.

Disclaimer. Publisher's note: Copernicus Publications remains neutral with regard to jurisdictional claims in published maps and institutional affiliations.

Acknowledgements. We thank the Captain and crew of the R/V *SA Agulhas II* for their support at sea and the Marine Biogeochemistry Lab in the Oceanography Department at the University of Cape Town for their assistance in the field and laboratory. We also thank the Flotilla Foundation and the Weddell Sea Expedition (2019). We thank Lija Treibergs, Reide Jacksin and Peter Ruffino for their assistance in analysing the nitrate isotopes and Riesna Audh for her assistance with satellite-derived sea ice concentration data. We thank Riesna Audh, Raquel Flynn and Shantelle Smith for nitrite concentration measurements and Raquel Flynn for quality controlling the nitrite concentration data.

Financial support. This research has been supported by a CAREER award to Julie Granger from the U.S. National Science Foundation (OCE-1554474). It has also been supported by the South African National Research Foundation through a Competitive Support for Rated Researchers Grant to Katye E. Altieri (111716) and a South African National Antarctic Programme Postgraduate Fellowship to Jessica Mary Burger and Grant to Katye E. Altieri (110732). Lastly this research was supported by the University of Cape Town through a University Research Council Launching Grant and VC Future Leaders 2030 Grant awarded to Katye E. Altieri.

Review statement. This paper was edited by Roya Bahreini and reviewed by two anonymous referees.

References

Alexander, B. and Mickley, L. J.: Paleo-perspectives on the potential future changes in the oxidative capacity of the atmosphere due to climate change and anthropogenic emissions, Current Pollution Reports, 1, 57–69, https://doi.org/10.1007/s40726-015-0006-0, 2015.

Alexander, B., Sherwen, T., Holmes, C. D., Fisher, J. A., Chen, Q., Evans, M. J., and Kasibhatla, P.: Global inorganic nitrate production mechanisms: comparison of a global model with nitrate isotope observations, Atmos. Chem. Phys., 20, 3859–3877, https://doi.org/10.5194/acp-20-3859-2020, 2020.

Altieri, K. E., Hastings, M. G., Gobel, A. R., Peters, A. J., and Sigman, D. M.: Isotopic composition of rainwater nitrate at Bermuda: the influence of air mass source and chemistry in the marine boundary layer, J. Geophys. Res.-Atmos., 118, 11304–11316, https://doi.org/10.1002/jgrd.50829, 2013.

Altieri, K. E., Fawcett, S. E., Peters, A. J., Sigman, D. M., and Hastings, M. G.: Marine biogenic source of atmospheric organic nitrogen in the subtropical North Atlantic, P. Natl. Acad. Sci. USA, 113, 925–930, https://doi.org/10.1073/pnas.1516847113, 2016.

Altieri, K. E., Fawcett, S. E., and Hastings, M. G.: Reactive Nitrogen Cycling in the Atmosphere and Ocean, Annu. Rev. Earth Pl. Sc., 49, 513–540, https://doi.org/10.1146/annurev-earth-083120-052147, 2021.

Atlas, E., Pollock, W., Greenberg, J., Heidt, L., and Thompson, A. M.: Alkyl nitrates, nonmethane hydrocarbons, and halocarbon gases over the equatorial Pacific Ocean during Saga 3, J. Geophys. Res., 98, 16933–16947, https://doi.org/10.1029/93JD01005, 1993.

Baker, A. R., Lesworth, T., Adams, C., Jickells, T. D., and Granzeveld, L.: Estimation of atmospheric nutrient inputs to the Atlantic Ocean from 50° N to 50° S based on large-scale field sampling: Fixed nitrogen and dry deposition of phosphorus, Global Biogeochem. Cy., 24, GB3006, https://doi.org/10.1029/2009GB003634, 2010.

Bauguitte, S. J.-B., Bloss, W. J., Evans, M. J., Salmon, R. A., Anderson, P. S., Jones, A. E., Lee, J. D., Saiz-Lopez, A., Roscoe, H. K., Wolff, E. W., and Plane, J. M. C.: Summertime NO_x measurements during the CHABLIS campaign: can source and sink estimates unravel observed diurnal cycles?, Atmos. Chem. Phys., 12, 989–1002, https://doi.org/10.5194/acp-12-989-2012, 2012.

Berhanu, T. A., Meusinger, C., Erbland, J., Jost, R., Bhattacharya, S. K., Johnson, M. S., and Savarino, J.: Laboratory study of nitrate photolysis in Antarctic snow. II. Isotopic effects and wavelength dependence, J. Chem. Phys., 140, 244306, https://doi.org/10.1063/1.4882899, 2014.

Berhanu, T. A., Savarino, J., Erbland, J., Vicars, W. C., Preunkert, S., Martins, J. F., and Johnson, M. S.: Isotopic effects of nitrate photochemistry in snow: a field study at Dome C, Antarctica, Atmos. Chem. Phys., 15, 11243–11256, https://doi.org/10.5194/acp-15-11243-2015, 2015.

Blake, N. J., Blake, D. R., Wingenter, O. W., Sive, B. C., Kang, C. H., Thornton, D. C., Bandy, A. R., Atlas, E., Flocke, F., Harris, J. M., and Rowland, F. S.: Aircraft measurements of the latitudinal, vertical, and seasonal variations of NMHCs, methyl nitrate, methyl halides, and DMS during the First Aerosol Characterization Experiment (ACE 1), J. Geophys. Res., 104, 21803–21817, https://doi.org/10.1029/1999JD900238, 1999.

Blake, N. J., Blake, D. R., Swanson, A. L., Atlas, E., Flocke, F., and Rowland, F. S.: Latitudinal, vertical, and seasonal variations of C_1-C_4 alkyl nitrate in the troposphere over the Pacific Ocean during PEM-Tropics A and B: Oceanic and continental sources, J. Geophys. Res., 108, 8242, https://doi.org/10.1029/2001JD001444, 2003.

Bölhke, J. K., Mroczkowski, S. J., and Coplen, T. B.: Oxygen isotopes in nitrate: new reference materials for ^{18}O:^{17}O:^{16}O measurements and observations on nitrate-water equilibrium, Rapid Commun. Mass Sp., 17, 1835–1846, https://doi.org/10.1002/rcm.1123, 2003.

Brough, N., Jones, A. E., and Griffiths, P. T.: Influence of sea ice-derived halogens on atmospheric HO_x as observed in Springtime coastal Antarctica, Geophys. Res. Lett., 46, 10168–10176, https://doi.org/10.1029/2019GL083825, 2019.

Burger, J. M., Granger, J., Joyce, E., Hastings, M. G., Spence, K. A. M., and Altieri, K. E.: The importance of alkyl nitrates and sea ice emissions to atmospheric NOx sources and cycling in the summertime Southern Ocean marine boundary layer, Version 3, Zenodo [data set], https://doi.org/10.5281/zenodo.5840260, 2021.

Casciotti, K. L., Sigman, D. M., Hastings, M. G., Böhlke, J. K., and Hilkert, A.: Measurement of the oxygen isotopic composition of nitrate in seawater and freshwater using the denitrifier method, Anal. Chem., 74, 4905–4912, https://doi.org/10.1021/ac020113w, 2002.

Chuck, A. L., Turner, S. M., and Liss, P. S.: Direct evidence for a marine source of C_1 and C_2 alkyl nitrates, Science, 297, 1151–1154, https://doi.org/10.1126/science.1073896, 2002.

Collett, K. S., Piketh, S. J., and Ross, K. E.: An assessment of the atmospheric nitrogen budget on the South African Highveld, S. Afr. J. Sci., 106, 1–9, https://doi.org/10.4102/sajs.v106i5/6.220, 2010.

Dahl, E. E. and Saltzman, S. E.: Alkyl nitrate photochemical production rates in North Pacific seawater, Mar. Chem., 112, 137–141, https://doi.org/10.1016/j.marchem.2008.10.002, 2008.

Dahl, E. E., Saltzman, S. E., and de Bruyn, W. J.: The aqueous phase yield of alkyl nitrates from ROO + NO: Implications for photochemical production in seawater, Geophys. Res. Lett., 30, 1271, https://doi.org/10.1029/2002GL016811, 2003.

Dahl, E. E., Yvon-Lewis, S. A., and Saltzman, S. E.: Saturation anomalies of alkyl nitrates in the tropical Pacific Ocean, Geophys. Res. Lett., 32, L20817, https://doi.org/10.1029/2005GL023896, 2005.

Dahl, E. E., Heiss, E. M., and Murawski, K.: The effects of dissolved organic matter on alkyl nitrate production during GOMECC and laboratory studies, Mar. Chem., 142, 11–17, https://doi.org/10.1016/j.marchem.2012.08.001, 2012.

Dar, S. S., Ghosh, P., Swaraj, A., and Kumar, A.: Craig–Gordon model validation using stable isotope ratios in water vapor over the Southern Ocean, Atmos. Chem. Phys., 20, 11435–11449, https://doi.org/10.5194/acp-20-11435-2020, 2020.

Davidson, E. A. and Kingerlee, W.: A global inventory of nitric oxide emissions from soils, Nutr. Cycl. Agroecosys., 48, 37–50, https://doi.org/10.1023/A:1009738715891, 1997.

Elliott, E. M., Kendall, C., Wankel, S. D., Burns, S. A., Boyer, E. W., Harlin, K., Bain, D. J., and Butler, T. J.: Nitrogen isotopes as indicators of NO_x source contributions to atmospheric nitrate deposition across the Midwestern and Northeastern United States, Environ. Sci. Technol., 41, 7661–7667, https://doi.org/10.1021/es070898t, 2007.

Erbland, J., Vicars, W. C., Savarino, J., Morin, S., Frey, M. M., Frosini, D., Vince, E., and Martins, J. M. F.: Air–snow transfer of nitrate on the East Antarctic Plateau – Part 1: Isotopic evidence for a photolytically driven dynamic equilibrium in summer, Atmos. Chem. Phys., 13, 6403–6419, https://doi.org/10.5194/acp-13-6403-2013, 2013.

Fang, Y. T., Koba, K., Wang, X. M., Wen, D. Z., Li, J., Takebayashi, Y., Liu, X. Y., and Yoh, M.: Anthropogenic imprints on nitrogen and oxygen isotopic composition of precipitation nitrate in a nitrogen-polluted city in southern China, Atmos. Chem. Phys., 11, 1313–1325, https://doi.org/10.5194/acp-11-1313-2011, 2011.

Finlayson-Pitts, B. J. and Pitts, J. N.: Chemistry of the upper and lower troposphere, Academic Press, San Diego, California, https://doi.org/10.1016/B978-0-12-257060-5.X5000-X, 2000.

Fisher, J. A., Atlas, E. L., Barletta, B., Meinardi, S., Blake, D. R., Thompson, C. R., Ryerson, T. B., Peischl, J., Tzompa-Sosa, Z. A., and Murray, L. T.: Methyl, ethyl and propyl nitrates: global distribution and impacts on reactive nitrogen in remote marine environments, J. Geophys. Res.-Atmos., 123, 12412–12429, https://doi.org/10.1029/2018JD029046, 2018.

Frey, M. M., Savarino, J., Morin, S., Erbland, J., and Martins, J. M. F.: Photolysis imprint in the nitrate stable isotope signal in snow and atmosphere of East Antarctica and implications for reactive nitrogen cycling, Atmos. Chem. Phys., 9, 8681–8696, https://doi.org/10.5194/acp-9-8681-2009, 2009.

Freyer, H. D., Kley, D., Volz-Thomas, A., and Kobel, K.: On the interaction of isotopic exchange processes with photochemical reactions in atmospheric oxides of nitrogen, J. Geophys. Res., 98, 14791–14796, https://doi.org/10.1029/93JD00874, 1993.

Freyer, H. D., Kobel, K., Delmas, R. J., Kley, D., and Legrand, M. R.: First results of $^{15}N/^{14}N$ ratios in nitrate from alpine and polar ice cores, Tellus B, 48, 93–105, https://doi.org/10.3402/tellusb.v48i1.15671, 1996.

Gobel, A. R., Altieri, K. E., Peters, A. J., Hastings, M. G., and Sigman, D. M.: Insights into anthropogenic nitrogen deposition to the North Atlantic investigated using the isotopic composition of aerosol and rainwater nitrate, Geophys. Res. Lett., 40, 5977–5982, https://doi.org/10.1002/2013GL058167, 2013.

Grannas, A. M., Jones, A. E., Dibb, J., Ammann, M., Anastasio, C., Beine, H. J., Bergin, M., Bottenheim, J., Boxe, C. S., Carver, G., Chen, G., Crawford, J. H., Dominé, F., Frey, M. M., Guzmán, M. I., Heard, D. E., Helmig, D., Hoffmann, M. R., Honrath, R. E., Huey, L. G., Hutterli, M., Jacobi, H. W., Klán, P., Lefer, B., McConnell, J., Plane, J., Sander, R., Savarino, J., Shepson, P. B., Simpson, W. R., Sodeau, J. R., von Glasow, R., Weller, R., Wolff, E. W., and Zhu, T.: An overview of snow photochemistry: evidence, mechanisms and impacts, Atmos. Chem. Phys., 7, 4329–4373, https://doi.org/10.5194/acp-7-4329-2007, 2007.

Grasshoff, K., Kremling, K., and Ehrhardt, M.: Methods of seawater analysis, Verlag Chemi, Florida, 1983.

Guilpart, E., Vimeux, F., Evan, S., Brioude, J., Mertzger, J., Barthe, C., Risi, C., and Cattani, O.: The isotopic composition of near-surface water vapor at the Maïdo observatory (Reunion Island, southwestern Indian Ocean) documents the controls of the humidity of the subtropical troposphere, J. Geophys. Res.-Atmos., 122, 9628–9650, https://doi.org/10.1002/2017JD026791, 2017.

Hamilton, D. S., Lee, L. A., Pringle, K. J., Reddington, C. L., Spracklen, D. V., and Carslaw, K. S.: Occurence of pristine aerosol environments on a polluted planet, P. Natl. Acad. Sci. USA, 111, 18466–18471, https://doi.org/10.1073/pnas.1415440111, 2014.

Hastings, M. G., Sigman, D. M., and Lipschultz, F.: Isotopic evidence for source changes of nitrate in rain at Bermuda, J. Geophys. Res., 108, 4790, https://doi.org/10.1029/2003JD003789, 2003.

Haywood, J. and Boucher, O.: Estimates of the direct and indirect radiative forcing due to tropospheric aerosols: a review, Rev. Geophys., 38, 513–543, https://doi.org/10.1029/1999RG000078, 2000.

Hoering, T.: The isotopic composition of the ammonia and the nitrate ion in rain, Geochim. Cosmochim. Ac., 12, 97–102, https://doi.org/10.1016/0016-7037(57)90021-2, 1957.

Hughes, C., Chuck, A. L., Turner, S. M., and Liss, P. S.: Methyl and ethyl nitrate saturation anomalies in the Southern Ocean (36–65° S, 30–70° W), Environ. Chem., 5, 11–15, https://doi.org/10.1071/EN07083, 2008.

IPCC: Boucher, O. D., Randall, P., Artaxo, C., Bretherton, G., Feingold, P., Forster, V.-M., Kerminen, Y., Kondo, H., Liao, U., Lohmann, P., Rasch, S.K., Satheesh, S., Sherwood, B., Stevens, and Zhang, X. Y.: Clouds and Aerosols, in: Climate Change 2013: The Physical Science Basis. Contribution of Working Group I to the Fifth Assessment Report of the Intergovernmental Panel on Climate Change, edited by: Stocker, T. F., Qin, D., Plattner, G.-K., Tignor, M., Allen, S. K., Boschung, J, Nauels, A., Xia, Y., Bex, V., and Midgley, P. M., Cambridge University Press, Cambridge, United Kingdom and New York, NY, USA, 2013.

Ishino, S., Hattori, S., Savarino, J., Jourdain, B., Preunkert, S., Legrand, M., Caillon, N., Barbero, A., Kuribayashi, K., and Yoshida, N.: Seasonal variations of triple oxygen isotopic compositions of atmospheric sulfate, nitrate, and ozone at Dumont d'Urville, coastal Antarctica, Atmos. Chem. Phys., 17, 3713–3727, https://doi.org/10.5194/acp-17-3713-2017, 2017.

Jiang, S., Shi, G., Cole-Dai, J., Geng, L., Ferris, D. G., An, C., and Li, Y.: Nitrate preservation in snow at Dome A, East Antarctica from ice core concentration and isotope records, Atmos. Environ., 213, 405–412, https://doi.org/10.1016/j.atmosenv.2019.06.031, 2019.

Jones, A. E., Weller, R., Minikin, A., Wolff, E. W., Sturges, W. T., McIntyre, H. P., Leonard, S. R., Schrems, O., and Bauguitte, S.: Oxidized nitrogen chemistry and speciation in the Antarctic troposphere, J. Geophys. Res., 104, 21355–21366, https://doi.org/10.1029/1999JD900362, 1999.

Jones, A. E., Weller, R., Wolff, E. W., and Jacobi, H.-W.: Speciation and rate of photochemical NO and NO_2 production in Antarctic snow, Geophys. Res. Lett., 27, 345–348, https://doi.org/10.1029/1999GL010885, 2000.

Jones, A. E., Weller, R., Anderson, P. S., Jacobi, H.-W., Wolff, E. W., Schrems, O., and Miller, H.: Measurements of NO_x emissions from the Antarctic snowpack, Geophys. Res. Lett., 28, 1499–1502, https://doi.org/10.1029/2000GL011956, 2001.

Kamezaki, K., Hattori, S., Iwamoto, Y., Ishino, S., Furutani, H., Miki, Y., Uematsu, M., Miura, K., and Yoshida, N.: Tracing the sources and formation pathways of atmospheric particulate nitrate over the Pacific Ocean using stable isotopes, Atmos. Environ., 209, 152–166, https://doi.org/10.1016/j.atmosenv.2019.04.026, 2019.

Kendall, C., Elliot, E. M., and Wankel, S. D.: Tracing anthropogenic inputs of nitrogen to ecosystems, in: Stable isotopes in ecology and environmental science, edited by: Michener, R. and Lajtha, K., Blackwell Publishing, Malden, Mass, 375–449, https://doi.org/10.1002/9780470691854.ch12, 2007.

Kroopnick, P. and Craig, H.: Atmospheric oxygen: isotopic composition and solubility fractionation, Science, 175, 54–55, 1972.

Lee, H.-M., Henze, D. K., Alexander, B., and Murray, L. T.: Investigating the sensitivity of surface-level nitrate seasonality in Antarctica to primary sources using a global model, Atmos. Environ., 89, 757–767, https://doi.org/10.1016/j.atmosenv.2014.03.003, 2014.

Michalski, G., Scott, Z., Kabiling, M., and Thiemens, M. H.: First measurments and modeling of $\Delta^{17}O$ in atmospheric nitrate, Geophys. Res. Lett., 30, 1870, https://doi.org/10.1029/2003GL017015, 2003.

Michalski, G., Bhattacharya, S. K., and Mase, D. F.: Oxygen isotope dynamics of atmospheric nitrate and its precursor molcules, in: Handbook of environmental isotope geochemistry. Advances in Isotope Geochemistry, edited by: Baskaran, M., Springer, Berlin, Heidelberg, 613–635, https://doi.org/10.1007/978-3-642-10637-8_30, 2012.

Monks, P. S.: Gas-phase radical chemistry in the troposphere, Chem. Soc. Rev., 34, 376–395, https://doi.org/10.1039/B307982C, 2005.

Morin, S., Savarino, J., Frey, M. M., Domine, F., Jacobi, H. W., Kaleschke, L., and Martins, J. M.: Comprehensive isotopic composition of atmospheric nitrate in the Atlantic Ocean boundary layer from 65° S to 79° N, J. Geophys. Res., 114, D05303, https://doi.org/10.1029/2008JD010696, 2009.

Nadzir, M. S., Ashfold, M. J., Khan, M. F., Robinson, A. D., Bolas, C., Latif, M. T., Wallis, B. M., Mead, M. I., Hamid, H. H. A., Harris, N. R. P., Ramly, Z. T. A., Lai, G. T., Liew, J. N., Ahamed, F., Uning, R., Samah, A. A., Maulud, K. N., Suparta, W., Zainudin, S. K., Wahab, M. I. A., Sahani, M., Müller , M., Yeok, F. S., Rahman, N. A., Mujahid, A., Morris, K. I., and Sasso, N. D.: Spatial-temporal variations in surface ozone over Ushuaia and the Antarctic region: observations from in situ measurements, satellite data, and global models, Environ. Sci. Pollut. R., 25, 2194–2210, https://doi.org/10.1007/s11356-017-0521-1, 2018.

Nesbitt, S. W., Zhang, R., and Orville, R. E.: Seasonal and global NO_x production by lightning estimated from the Optical Transient Detector (OTD), Tellus B, 52, 1206–1215, https://doi.org/10.3402/tellusb.v52i5.17098, 2000.

Park, S. S. and Kim, Y. J.: Source contributions to fine particulate matter in an urban atmosphere, Chemosphere, 59, 217–226, https://doi.org/10.1016/j.chemosphere.2004.11.001, 2005.

Park, Y., Park, K., Kim, H., Yu, S., Noh, S., Kim, M.-S, Kim, J.-Y., Ahn, J.-Y., Seok, K.-S., and Kim, Y.-H.: Characterizing isotopic compositions of TC-C, NO_3^--N and NH_4^+-N in $PM_{2.5}$ in South Korea: Impact of China's winter heating, Environ. Pollut., 233, 735–744, https://doi.org/10.1016/j.envpol.2017.10.072, 2018.

Rindelaub, J. D., McAvey, K. M., and Shepson, P. B.: The photochemical production of organic nitrates from α-pinene and loss via acid-dependent particle phase hydrolysis, Atmos. Environ., 100, 193–201, https://doi.org/10.1016/j.atmosenv.2014.11.010, 2015.

Rolph, G. D.: Real-time Environmental Applications and Display System (READY) Website, NOAA Air Resources Laboratory, College Park, MD, available at: https://www.ready.noaa.gov/index.php (last access: 12 January 2022), 2016.

Savarino, J., Kaiser, J., Morin, S., Sigman, D. M., and Thiemens, M. H.: Nitrogen and oxygen isotopic constraints on the origin of atmospheric nitrate in coastal Antarctica, Atmos. Chem. Phys., 7, 1925–1945, https://doi.org/10.5194/acp-7-1925-2007, 2007.

Scarchilli, C., Frezzotti, M., and Ruti, P. M.: Snow precipitation at four ice core sites in East Antarctica: provenance, seasonality and blocking factors, Clim. Dynam., 37, 2107–2125, https://doi.org/10.1007/s00382-010-0946-4, 2011.

Schumann, U. and Huntrieser, H.: The global lightning-induced nitrogen oxides source, Atmos. Chem. Phys., 7, 3823–3907, https://doi.org/10.5194/acp-7-3823-2007, 2007.

Shi, G., Buffen, A. M., Hastings, M. G., Li, C., Ma, H., Li, Y., Sun, B., An, C., and Jiang, S.: Investigation of post-depositional processing of nitrate in East Antarctic snow: isotopic constraints on photolytic loss, re-oxidation, and source inputs, Atmos. Chem. Phys., 15, 9435–9453, https://doi.org/10.5194/acp-15-9435-2015, 2015.

Shi, G., Buffen, A. M., Ma, H., Hu, Z., Sun, B., Li, C., Yu, J., Ma, T., An, C., Jiang, S., Li, Y., and Hastings, M. G.: Distinguishing summertime atmopsheric production of nitrate across the East Antarctic ice sheet, Geochim. Cosmochim. Ac., 231, 1–14, https://doi.org/10.1016/j.gca.2018.03.025, 2018.

Shi, G., Ma, H., Zhu, Z., Hu, A., Chen, Z., Jiang, Su., An, C., Yu, J., Ma, T., Li, Y., Sun, B., and Hastings, M. G.: Using stable isotopes to distinguish atmospheric nitrate production and its contribution to the surface ocean across hemispheres, Earth Planet. Sc. Lett., 564, 116914, https://doi.org/10.1016/j.epsl.2021.116914, 2021.

Sigman, D. M., Casciotti, K. L., Andreani, M., Barford, C., Galanter, M., and Böhlke, J. K.: A bacterial method for the nitrogen isotopic analysis of nitrate in seawater and freshwater, Anal. Chem., 73, 4145–4153, https://doi.org/10.1021/ac010088e, 2001.

Sinclair, K. E., Bertler, N. A. N., Trompetter, W. J., and Baisden, W. T.: Seasonality of airmass pathways to coastal Antarctica: ramifications for interpreting high-resolution ice core records, J. Climate, 26, 2065–2076, https://doi.org/10.1175/JCLI-D-12-00167.1, 2013.

Spreen, G., Kaleschke, L., and Heygster, G.: Sea ice remote sensing using AMSR-E 89-GHz channels, J. Geophys. Res., 113, C02S03, https://doi.org/10.1029/2005JC003384, 2008.

Stein, A. F., Draxler, R. R, Rolph, G. D., Stunder, B. J. B., Cohen, M. D., and Ngan, F.: NOAA's HYSPLIT atmospheric transport and dispersion modeling system, B. Am. Meteorol. Soc., 96, 2059–2077, https://doi.org/10.1175/BAMS-D-14-00110.1, 2015.

van der A, R. J., Eskes, H. J., Boersma, K. F., van Noije, T. P., Van Roozendael, M., De Smedt, I., Peters, D. H. M. U., and Meijer, E. W.: Trends, seasonal variability and dominant NO_x source derived from a ten year record of NO_2 measured from space, J. Geophys. Res., 113, D04302, https://doi.org/10.1029/2007JD009021, 2008.

Vicars, W. C. and Savarino, J.: Quantitative constraints on the ^{17}O-excess (Δ^{17}O) signature of surface ozone: Ambient measurements from 50° N to 50° S using the nitrite-coated filter technique, Geochim. Cosmochim. Ac., 135, 270–287, https://doi.org/10.1016/j.gca.2014.03.023, 2014.

Virkkula, A., Teinilä, K., Hillamo, R., Kerminen, V.-M., Saarikoski, S., Aurela, M., Viidanoja, J., Paatero, J., Koponen, I. K., and Kulmala, M.: Chemical composition of boundary layer aerosol over the Atlantic Ocean and at an Antarctic site, Atmos. Chem. Phys., 6, 3407–3421, https://doi.org/10.5194/acp-6-3407-2006, 2006.

Walters, W. W. and Michalski, G.: Theoretical calculation of nitorgen isotope equilibrium exchange fractionation factors for various NO_y molecules, Geochim. Cosmochim. Ac., 164, 284–297, https://doi.org/10.1016/j.gca.2015.05.029, 2015.

Walters, W. W. and Michalski, G.: Theoretical calculation of oxygen equilibrium isotope fractionation factors involving various NO_y molecules, OH, and H_2O and its implications for isotope variations in atmospheric nitrate, Geochim. Cosmochim. Ac., 191, 89—101, https://doi.org/10.1016/j.gca.2016.06.039, 2016.

Walters, W. W., Simonini, D. S., and Michalski, G.: Nitrogen isotope exchange between NO and NO_2 and its implications for δ^{15}N variations in tropospheric NO_x and atmospheric nitrate, Geophys. Res. Lett., 43, 440–448, https://doi.org/10.1002/2015GL066438, 2016.

Walters, W. W., Michalski, G., Bohlke, J. K., Alexander, B., Savarino, J., and Thiemens, M. H.: Assessing the seasonal dynamics of nitrate and sulfate aerosols at the South Pole utilizing stable isotopes, J. Geophys. Res.-Atmos., 124, 8161–8177, https://doi.org/10.1029/2019JD030517, 2019.

Weller, R., Jones, A. E., Wille, A., Jacobi, H.-W., McIntyre, H. P., Sturges, W. T., Huke, M., and Wagenback, D.: Seasonality of reactive nitrogen oxides (NO_y) at Neumayer Station, Antarctica, J. Geophys. Res., 107, 4673, https://doi.org/10.1029/2002JD002495, 2002.

Williams, J. E., Le Bras, G., Kukui, A., Ziereis, H., and Brenninkmeijer, C. A. M.: The impact of the chemical production of methyl nitrate from the NO + CH_3O_2 reaction on the global distributions of alkyl nitrates, nitrogen oxides and tropospheric ozone: a global modelling study, Atmos. Chem. Phys., 14, 2363–2382, https://doi.org/10.5194/acp-14-2363-2014, 2014.

Zong, Z., Wang, X., Tian, C., Chen, Y., Fang, Y., Zhang, F., Li, C., Sun, J., Li, J., and Zhang, G.: First assessment of NO_x sources at a regional background site in North China using isotopic analysis linked with modeling, Environ. Sci. Technol., 51, 5923–5931, https://doi.org/10.1021/acs.est.6b06316, 2017.